Multi-resolution Image Regression and Correlation to Track Natural Snowfalls over Extreme Spatial Extent

Koen Muller[1,*], Rafael Bölsterli[1,2], Doruk Alp Emür[1], Michael Lehning[3,4], and Filippo Coletti[1]

1: Institute of Fluid Dynamics, Mechanical and Process Engineering, ETH Zurich, Sonneggstrasse 3, 8092, Zurich, Switzerland
2: Strømningstekniske Laboratorier, Department of Energy and Process Engineering, Faculty of Engineering, NTNU, 229 Gløshaugen, Trondheim, Norway
3: Laboratory of Cryospheric Sciences, EPFL Valais Wallis, Route des Ronquos 86, 1951, Sion, Switzerland
4: Snow and Atmosphere, Snow Processes, WSL Institute for Snow and Avalanche Research (SLF), Flüelastrasse 11, 7260, Davos Dorf, Switzerland
*Corresponding author: kmuller@ethz.ch

Keywords: Natural Snowfall, Atmospheric Flows, Large-scale Field Experiments, UAVs, Two- and Three-dimensional Particle Tracking, Multi-resolution Image Wavelets

ABSTRACT

Harvesting real-world tracking data of natural snowfall requires performing large-scale field experiments beyond the reach of the laboratory and in the presence of challenging outdoor conditions at the limited capacity of available illumination. Utilizing a novel super-resolution field imaging system that combines 16 high-resolution cameras, we perform large-scale tracking of snowflakes falling through the atmospheric surface layer in two- and three-dimensions. Imaging snowfall over extreme spatial extents reveals snow images with diminishing contrast of only a few intensity counts, facing significant sources of nonuniform illumination. Moreover, imaging a large volumetric domain over a large depth of field presents significant magnification of snowflakes whose populations are inherently polydisperse in size and shape. To disentangle these combined effects of size, shape, and magnification in the presence of significant noise, we apply a multi-resolution image regression. Essentially, our methodology integrates a Savitzky-Golay interpolation kernel into a multi-resolution image wavelet basis that sequentially decomposes the image in layers, fitting Gaussians of unknown size and shape for particle identification. Assigning a color space to the image decomposition layers, we show how our methodology reveals the spectral content of the image, helps discern small and large snow particles, and provides control over out-of-focus images in the foreground and noise rejection. Integrating a Delaunay triangulation, we devise a multidimensional tracking assignment among different scale layers and obtain tracking vectors through a topological image correlation. We showcase the application of our methodology to snow particle tracking obtained from two field experiments. First, we reveal large-scale snowfall structures with a wavy streamwise flow in a planar snow tracking experiment, for which we recover the logarithmic law of the wall, and whose wavenumber spectrum reveals signatures of rapid distortion. Secondly, performing volumetric tracking, we match snow particles over a large depth of field and scale up Voronoi analysis over previous advances, revealing a predominance of snow clustering and voids over a random Poisson process, as well as an apparent multi-modality in the snow fall speed.

1. Introduction

The interactions between large collections of precipitating snowflakes in the presence of various turbulence intensity levels over the air column make snowfalls difficult to forecast. Understanding their complex multi-scale inertial clustering dynamics (Brandt & Coletti, 2022) is key to understanding spatial modulations in the snow deposition process during precipitation (Guala & Hong, 2025), and to interpret remote sensing signals.

We utilize a novel super-resolution field experimental setup that combines 16 cameras to perform large-scale field tracking of snowflakes falling through the atmospheric surface layer in the Swiss Alps. Our work significantly scales up snowfall tracking over previous advances in two- (Heisel et al., 2018; Li et al., 2021) and three-dimensional field imaging (Bristow et al., 2023; Li et al., 2024; Lungo et al., 2024). Arranging our camera system in a linear configuration, we image up to a $60 \times 15\,\mathrm{m}^2$ field of view, enabling the characterization of the space-time variability of snow in the atmosphere. Arranging our camera system in a semi-circular arc, we overlap a $10 \times 10 \times 10\,\mathrm{m}^3$ measurement volume, leveraging the tracking of millions of snowflakes in three dimensions.

Imaging snowfall over such extreme spatial extents presents significant sources of nonuniform illumination, resulting in snow images with diminishing contrast of only a few intensity counts, presenting a signal-to-noise ratio of order unity, well within the range of the image noise floor. Moreover, imaging snow over a large depth of field using wide-angle lenses can result in significant magnification of snowflakes whose populations are polydisperse in size and shape (Garrett & Yuter, 2014; Rees et al., 2021), in turn affecting their fall speed and behavior.

In this work, we disentangle these combined effects of size, shape, and magnification in the presence of significant noise by a multi-resolution image regression to devise a multi-dimensional tracking assignment. Essentially, our methodology integrates a Savitzky-Golay-based particle interpolation kernel (Meer & Weiss, 1992; Nobach & Honkanen, 2005) into a multi-resolution image wavelet basis (Daubechies, 1992; Mallat, 2009) to sequentially decompose the image into layers, fitting Gaussians of unknown size and shape at increasing scale. Assigning a color space to the image decomposition layers, we show how our methodology reveals the spectral content of the image, helps discern small and large snowflakes, and provides control over out-of-focus particles in the foreground and noise rejection. Integrating a Delaunay triangulation among different scale layers, we explain how we obtain tracking vectors through a topological image correlation.

We showcase the application of our methodology to particle tracking data from two field experimental deployments. In a first deployment, we perform planar imaging to track snowfall over a long streamwise extent. We recover the logarithmic law of the wall (Heisel et al., 2018) and reveal large-scale snowfall structures with a wavy flow whose spectrum shows signatures of rapid distortion (Hunt & Carlotti, 2001). In a second deployment, we perform volumetric imaging. We integrate extracted geometric information in matching snowflakes over large distances and scale

up Voronoi analysis from previous advances (Bristow et al., 2023). Our results show a predominance of snow clustering and an apparent multi-modality in the snow fall speed, whose origins can be influenced by several factors, including interactions with vortical structures in the atmosphere.



Figure 1. Large-scale field experimental setup. a) Field deployment imaging snow from ice-fishing tents that surround a powerful stadium illumination deployed for volumetric imaging. b) Single camera array, hosting 4 high-resolution cameras in a shift-lens configuration to construct a large field of view.

2. Field Experimental Setup

Our field experimental setup combines 16 high-resolution $25\,\mathrm{MP}$ area scan machine vision cameras (IRON0505, KAYA INSTRUMENTS) mounted on 2-by-2 arrays, see Figure 1. Each camera array is fitted with shifted wide-angle lenses ($22\,\mathrm{mm}$ $\mathrm{f}/1.4$, SAMYANG) to stitch an equivalent $100\,\mathrm{MP}$ imaging over a $20 \times 20\,\mathrm{m}^2$ field of view, with a depth of field of $26\,\mathrm{m}$ at a $2\,\mathrm{mm}$ diffraction-limited tracking resolution (Adrian, 1991). Snowflakes are illuminated using white light of $5500\,\mathrm{K}$ at $250'000\,\mathrm{lm}$ from multiple powerful $1575\,\mathrm{W}$ stadium floodlight panels (BIG287000, PLAYLED) mounted on snowboards and retrofitted with lenticular lenses and blinders. Shooting data at $150\,\mathrm{Hz}$, the system is capable of imaging snowfall at 1 terabit-per-second and tracking millions of snowflakes simultaneously.

The imaging system is flexibly deployed in ice-fishing tents at an instrumented field site that collocates a meteorological tower. Our field imaging system can be arranged in two configurations. When configured in a line, the cameras stitch a $400\,\mathrm{MP}$ image over a maximum $60 \times 15\,\mathrm{m}^2$ field of view, illuminating snowfall over a 1-meter thick slab, for which the cameras are calibrated by the GPS path of a DJI MAVIC 3E drone with a spotlight (GL10, CZZI). When configured in a

semi-arc, the cameras overlap a $10 \times 10 \times 10\,\mathrm{m}^3$ measurement volume surrounding a cubic illumination, and the cameras are calibrated using a larger DJI MATRICE 300 drone that carries four bright calibration markers arranged in a known geometry.

3. Multi-resolution Image Regression

Figure 2a shows a typical field experimental image obtained for a large-scale snow tracking experiment. Spreading the illumination over a vast volumetric range reveals snowfall within a severely nonuniform illumination, showing a diminishing image contrast that attenuates into the range of the image noise floor. In addition, it can be observed that snowflakes significantly magnify over the depth of field, including out-of-focus particles outside the measurement volume and close to the camera.

To identify various snow particles in the presence of these artifacts, we consider their projections as simple projections of Gaussian intensity with unknown size and shape. To find their unknown parametrizations in the image I_{ij} with coordinates $\mathbf{x} = [x\ y]^T$ and pixel indices ij, we integrate a second-order particle interpolation kernel (Nobach & Honkanen, 2005) into a multi-resolution image regression by fitting polynomial basis-function expansion to a prescribed local pixel neighborhood ij^* with Gaussian weighting function w_{ij^*}:

$$\min_{c_k^s} \sum_{s=1}^{S} \sum_{ij^*} w_{ij^*}^s \left(I_{ij^*}^s - \sum_{z=s}^{S} \sum_{k=0}^{K} c_k^z \phi_k \left(\mathbf{x}_{ij^*} \right) \right)^2 \ \forall ij \text{ with } w_{ij^*}^s = \exp\left(-\frac{1}{2} \left(\frac{\|\mathbf{x}_{ij^*}\|}{\sigma^s} \right)^2 \right). \tag{1}$$

Here $\phi_k(\mathbf{x}) = x^l y^h \ \forall\ lh \leq 2$ describe a contour function $f(\mathbf{x}) = \sum_{k=0}^{K} c_k \phi_k(\mathbf{x}) = 0$ with unknown coefficients c_k that vary over increasing scales s with growth factor σ. This image filter design is used to sequentially decompose the image I_{ij} in layers s by subtracting extracted coefficient information $c_0^s|_{ij}$ from the preceding layers up to $s-1$ to correct $I_{ij}^s = I_{ij} - \sum_{z=0}^{s-1} c_0^z \big|_{ij}$.

Essentially Equation 1 presents multi-resolution image wavelet decomposition (Daubechies, 1992; Mallat, 2009), which is projected onto a set of polynomial coefficients that optimally fit to the image (Meer & Weiss, 1992), locally weighted on its Gauss-stencil. Where multi-resolution wavelet filters are known to be robust against noise, their sparse representations can be used for image segmentation and particle identification in the current application. Vectorizing Equation 1 allows deriving a set of linear convolution filters that are separable, and can be efficiently implemented in the frequency domain and/or using pyramids.

To apply the image regression to raw image data, we first subtract an image background that is patched from the minimum pixelwise intensity over time, and corrected for instantaneous row-column sensor noise. In Figure 2b, we apply the image decomposition for a total of eight consecutive layers for four cameras on a single array. Projecting the decomposition on an RGB color-space, we reveal the spectral image content, which can be used to discern small snowflakes in

the background (blue) from larger ones in the foreground (yellow), see inset. In addition, we further remove blurred snow particles close to the camera by omitting the last layer. Finally, in Figure 2b, we show the image residual that can be used for noise rejection in split view with the input background-subtracted image.

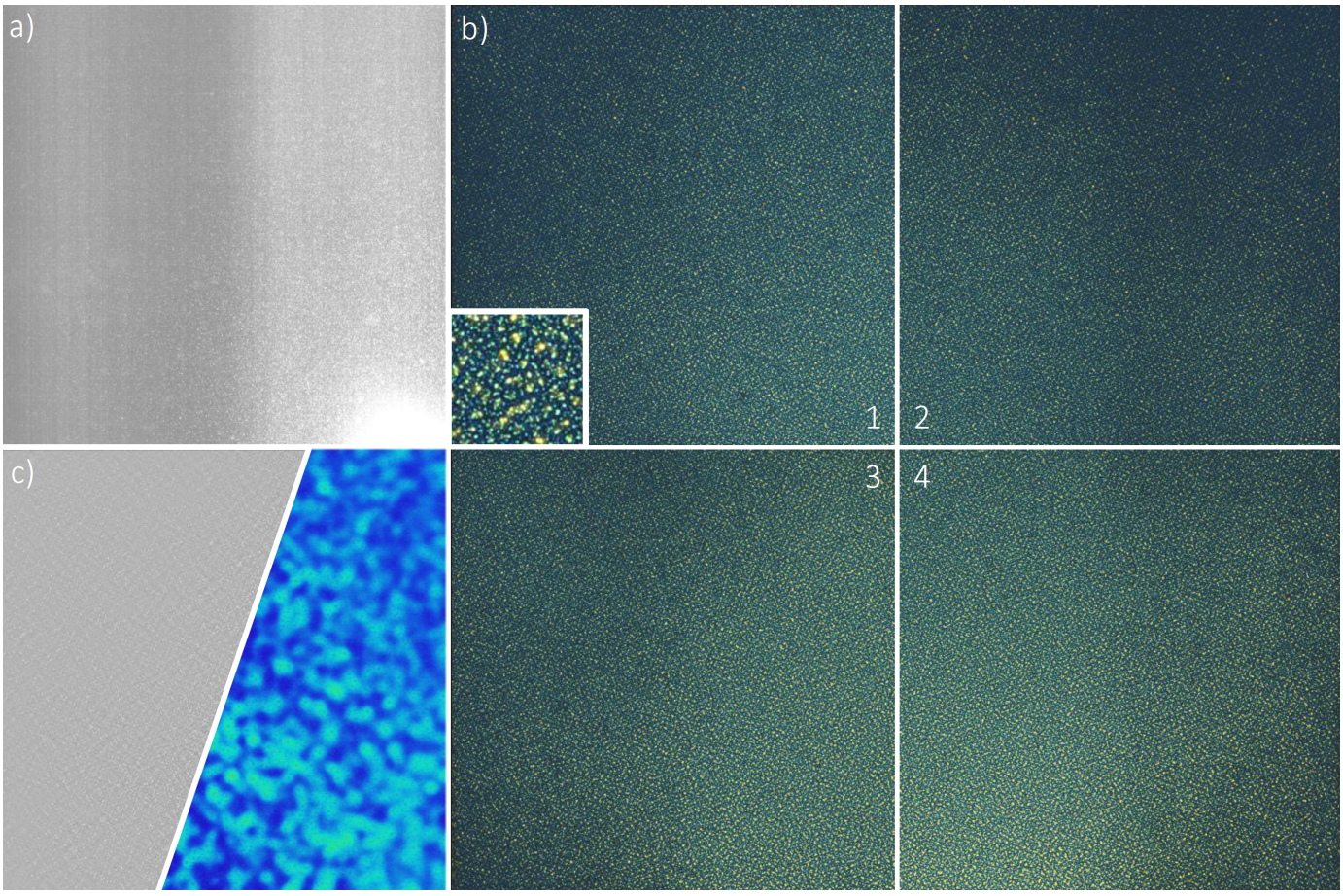


Figure 2. Multi-resolution image regression. a) Raw camera image, revealing nonuniform illumination and significant sources of noise. b) Scale decomposed image for the 2-by-2 camera array, showing the spectral image content. Insert a zoomed-in image showing small snowflakes in blue and larger ones in yellow. c) Split view of the background-subtracted image and its image residual from fitting the multi-resolution image filter design.

4. Delaunay-based Image Correlation

From image decomposition, we identify snow particles p by segmenting those pixelwise coefficient data $c_k^s|_{ij}$ whose contour functions satisfy local peak images, and label their centroid locations that cluster near the same pixels. From the labeled coefficient data $c_k^s|_{ij}^p$ we subsequently compute the average contour function of the snow particle as the coefficient vector $\mathbf{c}_p$ in the image coordinates $\mathbf{x}$. The labeled coefficient data $c_0^s|_{ij}^p$ presents a sparse representation of pixel intensity that contains snow particles in the scale-decomposed image, providing a unique finderprint to each snow

particle identification. We now use this representation to define a multidimensional tracking assignment over the different layers s between consecutive image frames through image correlation.

First, we construct a three-dimensional Delaunay triangulation between snow particles p in frame n and snow particles q in frame $n+1$ given a layer s. This defines an undirected graph $G(V, E)$ with the vertices V at the p, q particle positions and edges E between them. Within the separate image frames, the edges E interconnect nearest neighbors for p and q, which we denote as the sets pp and qq. Between the separate image frames, the edges E provide candidate tracking matches between p and q, which we denote as the set pq. Looping the different scales layers s and branching prescribed generations over the edges E, we accumulate pp, qq nearest neighbors and pq tracking candidates, which are stored as indexed lists.

To find the best tracking vectors $\mathbf{u} = [u\ v]^T$ among the candidate tracking matches pq between frames n and $n+1$, we write down a weighted image correlation for the scale decomposed intensity $c_0^s|_{ij}^p$ and $c_0^s|_{ij}^q$ for the particle images p and q:

$$\max_{u,v \in pq} \sum_{ijs} \sum_{p \in pp} w_p c_0^s|_{i-u,j-v}^p \sum_{q \in qq} w_q c_0^s|_{ij}^q. \tag{2}$$

Here $\sum_{p \in pp} w_p c_0^s|_{ij}^p$ and $\sum_{q \in qq} w_q c_0^s|_{ij}^q$ construct local image neighborhoods for the particle pairs pq from branching their nearest neighbors pp and qq whose relative importance are weighted by their Pearson similarity $w_{p\ (\text{or}\ q)}$.

The image correlation statement rewards spatially correlated tracking vectors that optimally fit snowflakes of different sizes and shapes from one image to the next. At first hand, this statement may appear intractable to solve for the unknown tracking vector $\mathbf{u}$, requiring constructing custom interrogation around each snow particle p and q and summing over all scale layers s. However, recognizing that pp, qq, and pq are known over the scale layers s, we implement Equation 2 as a topological particle tracking that branches locally over the Delaunay-graph by writing the image correlation as a sparse banded matrix operator.

In Figure 3a, we showcase eight times zoomed-in snow identification images with their Delaunay triangulation among three consecutive scale layers s. In Figure 3b, c, and d, we show the resulting image identification, the extracted Delaunay graph for tracking, and the resulting tracking vectors for a single frame pair, respectively. Through this procedure, we obtain a large number of image identifications and tracking vectors that can be used for correspondence matching between views and tracking over image frames.

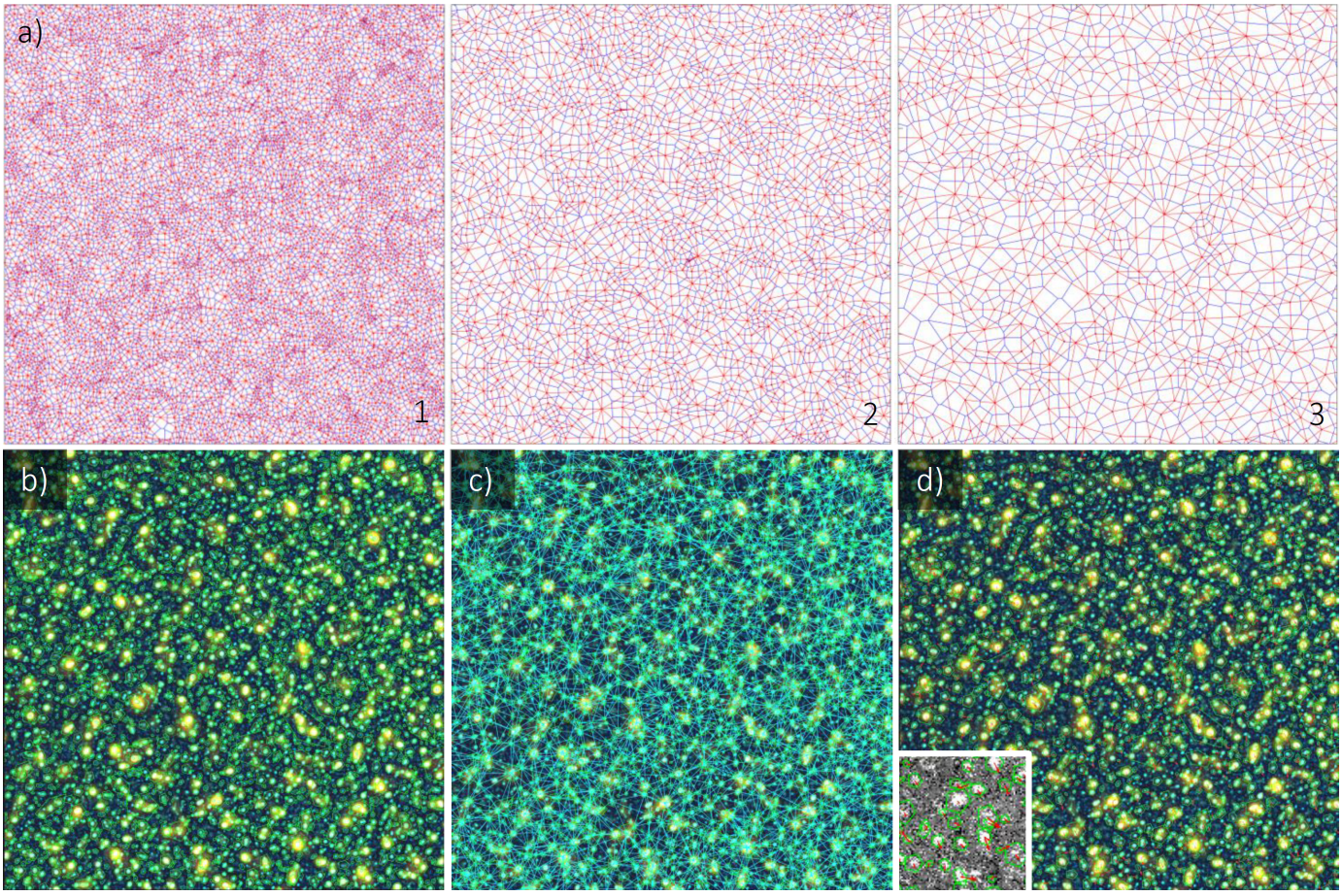


Figure 3. Topological tracking on the Delaunay-graph. a) Extracted Delaunay triangulation (red) over several consecutive scale layers for a single frame with complementary Voronoi tesselation in blue. b) Snow particle identification, rendering the extracted contour function as 5-point polygons. c) Delaunay graph used to construct the tracking neighborhood around each snow particle. d) Tracking vectors obtained through optimizing the image correlation. Inset at bottom left, zoomed sample on the background-subtracted image.

5. Application to Field Experiments of Natural Snowfall

Having explained our image processing and multi-dimensional tracking assignment, we now proceed to apply the methodology to field experimental snow tracking data. We first apply our methodology to a planar imaging of snowfall over a large streamwise extent to resolve the spatial-temporal transport of snow in the atmosphere. Secondly, we apply our image processing to volumetric tracking of snowfall, where we use the extracted contour function to match and track particles among different views.

5.1. Planar Boundary Layer Evolution

In Figure 4, we show planar snowfall tracking results for a $1/2$-second time window realizing a $50 \times 15\,\mathrm{m}^2$ field of view by overlapping 16 cameras in a linear configuration*. Applying our multi-resolution image processing and correlation methodology, we obtain snow trajectories over the full extent of three stadium illumination panels positioned beneath the snowfall and between the camera arrays. The results reveal a surprisingly wavy snowfall pattern, which is further exaggerated when integrating streamlines over the extracted flowfield that is obtained by spatially binning the snowfall trajectory data.

Spatio-temporally averaging the flow along the streamwise direction reveals results consistent with the logarithmic law of the wall profile for an atmospheric boundary layer:

$$\bar{u}(z) = \frac{u_\star}{\kappa} \ln\left(\frac{z}{z_0}\right), \tag{3}$$

with von Kármán-constant $\kappa = 0.4$, and where we obtain $u_\star = 0.2362\,\mathrm{m/s}$ and a roughness parameter of $z_0 = 0.0044\,\mathrm{m}^\dagger$ (Heisel et al., 2018). Furthermore, for the observed wavy flow structure, we find inversely proportional power-law scalings ${k_x}^{-\gamma}$ for streamwise wavenumber spectrum with $\gamma = 1$ up to wavelengths of $\lambda \simeq 4.2$ and $8.4\,\mathrm{m}$ which reveal signatures of rapid distortion theory (Hunt & Carlotti, 2001), preceeding higher wavenumbers with scaling exponent $\gamma = 5/3$ into the inertial subrange.

5.2. Volumetric Snow Clustering Dynamics

In Figure 5, we show results for three-dimensional snowfall imaging, realizing tracking over $700'000$ snowflakes over a $10 \times 10 \times 10\,\mathrm{m}^3$ cubic measurement volume. To match snow particles over a large depth of field, we encode the optical transfer (Schanz et al., 2013) between the image and object through the contour function whose geometry is naturally embedded in projective geometry (Hartley & Zisserman, 2003). Furthermore, using the extracted tracking vector, we only track those matches that remain in consistent correspondence between frames, as is conventional in state-of-the-art tracking methodologies such as the 'Shake-the-Box'-algorithm (Schanz et al., 2016).

Finally, we scale up snow clustering analysis over a thousand cubic meters. Following Bristow et al. (2023), we sample Vonoroi-cells of volume $\mathcal{V}$ to analyse the degree of snow clustering compared to a random point Poisson process:

$$f\left(\mathcal{V}^*\right) = \nu {\mathcal{V}^*}^4 \exp\left(-5\mathcal{V}^*\right), \tag{4}$$

with reduced $\mathcal{V}^* = \mathcal{V}/\langle\mathcal{V}\rangle$, and normalization factor $\nu = 3125/24$ (Ferenc & Néda, 2007). In Figure 5d, we find a predominance of clustering and voids sampling well above the reference

*Appreciating some misalignment for the first camera array.

†Corresponding to an actual roughness in range of $\sim 20\,\mathrm{cm}$.

curve, while in Figure 5e we find an apparent multi-modality in the fall speed, with a significant amount of slow (blue), average (cyan), and some fast (yellow/red) falling trajectories. Both of these results are signatures of non-trivial clustering mechanisms of snowflakes in interaction with vortical structures in the turbulent atmosphere.

6. Conclusions

We presented a multi-resolution image regression and correlation to track natural snowfall over an extreme spatial extent. Essentially, our methodology integrates a Savitzky-Golay image interpolation kernel into a multi-resolution image wavelet basis, projecting it onto an image decomposition that fits optimally to the image and reveals its spectral content. From this decomposition, we devised a multi-dimensional tracking assignment by writing down the image correlation between consecutive frames that branches locally over the topology of the Delaunay triangulation graph.

We demonstrated the application of our methodology to large-scale field experiments of natural snowfall, performing imaging in the presence of nonuniform illumination and significant noise. Applying our methodology to planar tracking, we revealed wavy snowfall trajectories in planar imaging over a long streamwise extent, recovered the logarithmic law of the wall, and found signatures of rapid distortion theory. Applying our methodology to volumetric tracking, we used the image decomposition to discern small and large snowflakes over a large depth of field. scaling up imaging over previous advances, we revealed a predominance of clustering and voids tracking over $700'000$ snowflakes simultaneously over a thousand cubic meters.

In future work, we aim to further apply well-established and state-of-the-art tracking methodologies such as the Shake-the-Box algorithm. At the conference, we will further assess the robustness of the approach by sampling synthetic data.

Acknowledgements

The authors would like to acknowledge support from the Swiss National Science Foundation (SNSF) under project No. 200021_212065 and the Dutch Organisation for Scientific Research (NWO) Rubicon grant project No. 019.233EN.018. We particularly thank Sergi Gonzàlez-Herrero, Ivan Calic, Pim Bullee, Alessandro Gambino, Udhav Gawandalkar, Yifan Wang, and Sebastian Käser for their assistance during the field measurement campaigns.

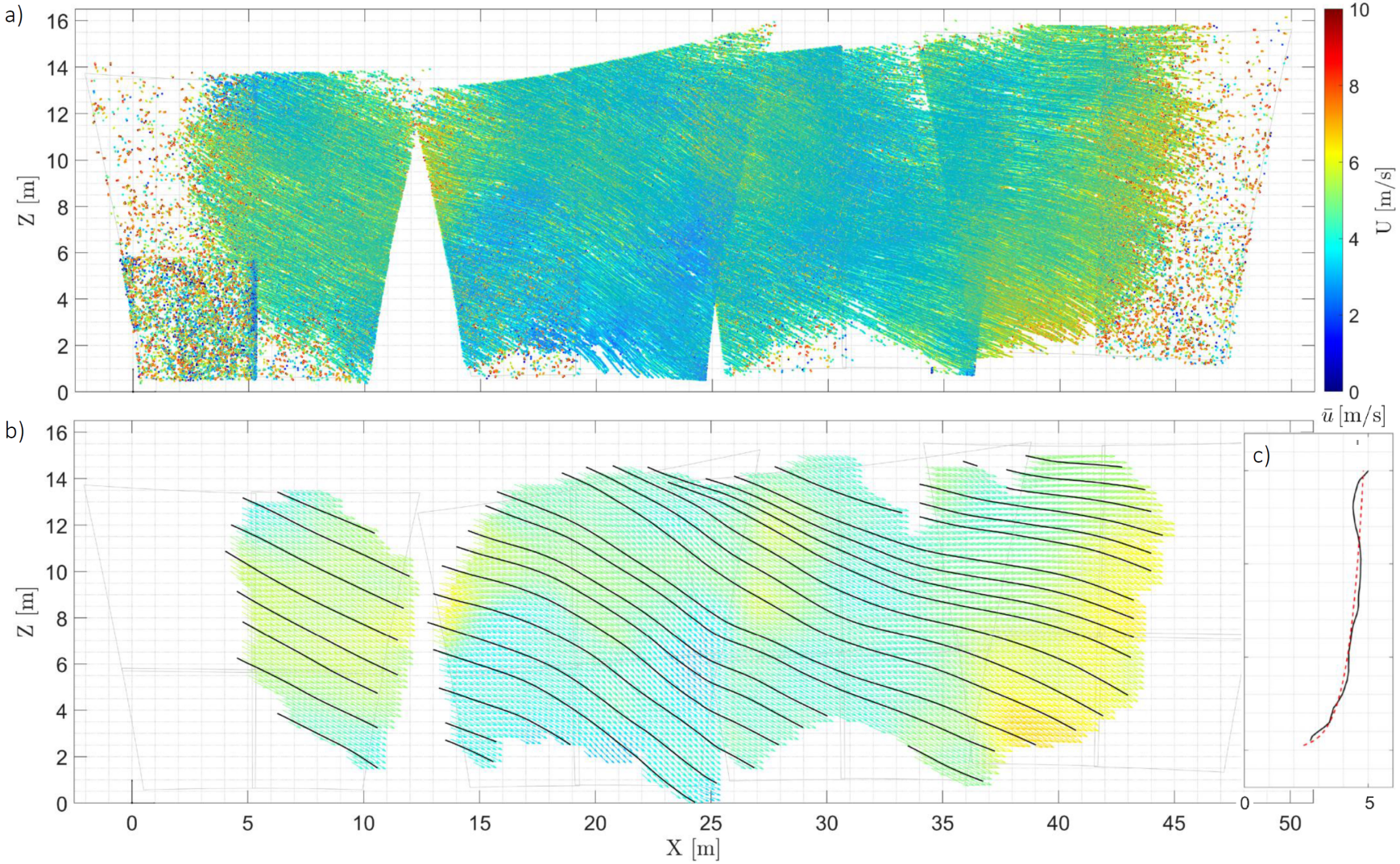


Figure 4. Planar snowfall tracking. a) Snowfall trajectories over a long streamwise extent spanning a $50 \times 15\,\mathrm{m}^2$ field of view, revealing a wavy snowfall pattern color-coded for the linear velocity. b) Extracted flow field, regressing a flow map over $0.5 \times 0.5\,\mathrm{m}^2$ grid bins with a regular spacing of 0.25 m and sampling several streamlines in black. At the right-hand side, we inset (c) a fitted logarithmic law of the wall profile (red dashed) to the streamwise spatio-temporally averaged flow $\bar{u}(z)$ in black.

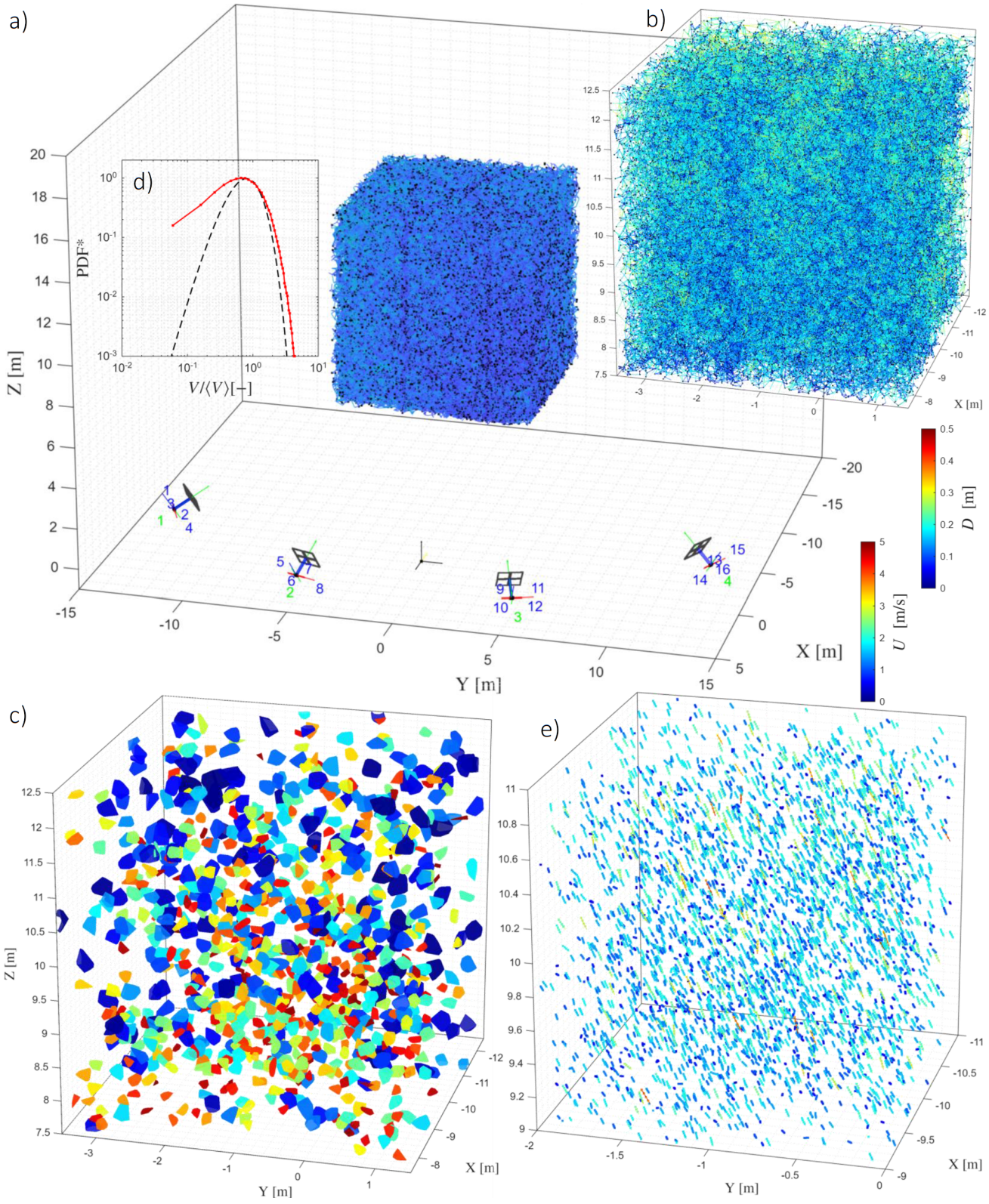


Figure 5. Volumetric snowfall tracking. a) Calibrated camera setup tracking over 700′000 snowflakes from 16 cameras on arrays intersecting a large volumetric domain of $10 \times 10 \times 10\,\mathrm{m}^3$. b) Zoomed volume of $5 \times 5 \times 5\,\mathrm{m}^3$ color-coding a Delaunay triangulation for the interparticle distance D. c) Sparse sampling of Voronoi-cells showing small (red) and large volumes (blue). d) Clustering diagram, revealing predominance of clusters and voids in red. e) Snowflake tracking over a $2 \times 2 \times 2\,\mathrm{m}^3$ subvolume, showing various color-codes for the linear velocity.

References

Adrian, R. J. (1991). Particle-imaging Techniques for Experimental Fluid Mechanics. *Annu. Rev. Fluid Mech*, *23*, 261–304. Retrieved from www.annualreviews.org

Brandt, L., & Coletti, F. (2022). Particle-Laden Turbulence: Progress and Perspectives. *Annu. Rev. Fluid Mech. 2022*, *54*, 159–189. Retrieved from https://doi.org/10.1146/annurev-fluid-030121- doi: 10.1146/annurev-fluid-030121

Bristow, N., Li, J., Hartford, P., Guala, M., & Hong, J. (2023, 10). Imaging-based 3D Particle Tracking System for Field Characterization of Particle Dynamics in Atmospheric Flows. *Experiments in Fluids*, *64*(78). Retrieved from http://arxiv.org/abs/2210.07106 doi: 10.1007/s00348-023-03619-6

Daubechies, I. (1992). *Ten Lectures on Wavelets*. Society for Industrial and Applied Mathematics.

Ferenc, J. S., & Néda, Z. (2007, 11). On the size distribution of Poisson Voronoi cells. *Physica A: Statistical Mechanics and its Applications*, *385*(2), 518–526. Retrieved from https://www.sciencedirect.com/science/article/pii/S0378437107007546 doi: 10.1016/J.PHYSA.2007.07.063

Garrett, T. J., & Yuter, S. E. (2014, 9). Observed influence of riming, temperature, and turbulence on the fallspeed of solid precipitation. *Geophysical Research Letters*, *41*(18), 6515–6522. doi: 10.1002/2014GL061016

Guala, M., & Hong, J. (2025). Snow Settling in Atmospheric Turbulence. *Annual Review of Fluid Mechanics Downloaded from www.annualreviews.org. ETH Zurich*, *23*. Retrieved from https://doi.org/10.1146/annurev-fluid-112823- doi: 10.1146/annurev-fluid-112823

Hartley, R., & Zisserman, A. (2003). *Multiple view geometry in computer vision* (2nd ed.). Cambridge: Cambridge University Press.

Heisel, M., Dasari, T., Liu, Y., Hong, J., Coletti, F., & Guala, M. (2018, 12). The spatial structure of the logarithmic region in very-high-Reynolds-number rough wall turbulent boundary layers. *Journal of Fluid Mechanics*, *857*, 704–747. doi: 10.1017/jfm.2018.759

Hunt, J. C., & Carlotti, P. (2001). Statistical Structure at the Wall of the High Reynolds Number Turbulent Boundary Layer. *Flow, Turbulence and Combustion*, *66*, 453–475.

Li, J., Abraham, A., Guala, M., & Hong, J. (2021, 12). Evidence of preferential sweeping during snow settling in atmospheric turbulence. *Journal of Fluid Mechanics*, *928*. doi: 10.1017/jfm.2021.816

Li, J., Guala, M., & Hong, J. (2024, 8). Field investigation of 3D snow settling dynamics under weak atmospheric turbulence. *Journal of Fluid Mechanics*, *997*, 1–33. Retrieved from `http://arxiv.org/abs/2406.08737`

Lungo, G. V., Guala, M., Hong, J., Bristow, N., Puccioni, M., Hartford, P., … Moss, C. (2024, 1). Grand-Scale Atmospheric Imaging Apparatus (GAIA) and Wind Lidar Multiscale Measurements in the Atmospheric Surface Layer. *Bulletin of the American Meteorological Society*, *105*(1), E121-E143. doi: 10.1175/BAMS-D-23-0066.1

Mallat, S. (2009). *A Wavelet Tour of Signal Processing: The Sparse Way*. Academic Press.

Meer, P., & Weiss, I. (1992, 6). Smoothed differentiation filters for images. *Journal of Visual Communication and Image Representation*, *3*(1), 58–72. Retrieved from `https://doi.org/10.1016/1047-3203(92)90030-W` doi: 10.1016/1047-3203(92)90030-W

Nobach, H., & Honkanen, M. (2005, 4). Two-dimensional Gaussian regression for sub-pixel displacement estimation in particle image velocimetry or particle position estimation in particle tracking velocimetry. *Experiments in Fluids*, *38*(4), 511–515. doi: 10.1007/s00348-005-0942-3

Rees, K. N., Singh, D. K., Pardyjak, E. R., & Garrett, T. J. (2021, 9). Mass and density of individual frozen hydrometeors. *Atmospheric Chemistry and Physics*, *21*, 14235–14250. doi: 10.5194/acp-21-14235-2021

Schanz, D., Gesemann, S., & Schröder, A. (2016). Shake-The-Box: Lagrangian particle tracking at high particle image densities. *Experiments in Fluids*, *57*, 1–27. doi: 10.1007/s00348-016-2157-1

Schanz, D., Gesemann, S., Schröder, A., Wieneke, B., & Novara, M. (2013). Non-uniform optical transfer functions in particle imaging: Calibration and application to tomographic reconstruction. *Measurement Science and Technology*, *24*(2). doi: 10.1088/0957-0233/24/2/024009